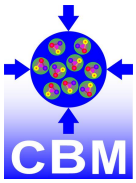

COMPRESSED BARYONIC MATTER EXPERIMENT

CBM-TN-22008
May 8, 2023

Impact of air cooling on the mechanical stability of silicon sensors for CBM STS

S. Mehta*[1], K. Agarwal[1], U. Frankenfeld[2], J. M. Heuser[1,2], F. Nickels[2], H. R. Schmidt[1,2], G. Viehhauser[3]

[1] Eberhard Karls University of Tübingen, Germany
[2] GSI Helmholtzzentrum für Schwerionenforschung GmbH, Darmstadt, Germany
[3] University of Oxford, Oxford, United Kingdom

*Email: s.mehta@gsi.de

Abstract

This note investigates the influence of forced air cooling on the mechanical stability of the silicon sensors assembled on the ladder. The study involves exposing a fully assembled ladder to controlled airflow using a perforated tube that directs cold air onto the sensor's surface. The objective is to examine the vibrations caused by the air flow and their effect on sensor stability and tracking efficiency of the STS. The vibrations induced by the airflow were precisely measured and analysed to determine their effects on the mechanical integrity of the silicon sensors. Additionally, the resulting vibrations were examined to identify any observable relationship between sensor stability and tracking performance.

Table of Contents

1 Introduction to cooling concept

The carbon fiber ladders used in STS are lightweight structures designed to provide high rigidity [1]. These structures supports the modules comprising of sensors connected to front-end electronics via the micro cables. The front-end electronics dissipate an estimated power of 40 kW with power dissipated by each FEB $\sim$ 20 W. Additionally, the silicon sensors in the STS are exposed to high radiation environment, reaching exposure levels of up to 10^{14} n_{eq}/cm^2, especially for the sensors close to the beam pipe. These sensors with $\Delta x = \Delta y \leq 10$ cm, are subjected to the highest radiation dose, producing up to 7 mW/cm^2 at -10°C. To prevent thermal runaway and effectively dissipate the resulting excess heat, active air cooling is crucial. By employing active air cooling specifically for the sensors located in the high radiation zone, the STS ensures that the temperature remains within acceptable limits, preserving the performance and longevity of the sensors.

To minimize the impact on the detector geometry and material budget, a cooling concept with low material budget is selected for the cooling of central sensors in STS. Perforated tubes,based on the "Impinging jets" concept, will be used as the cooling element. Cold and dry nitrogen will be blown directly onto the surface of the sensors, specifically targeting the innermost sensors, for efficient heat removal [2]. These tubes, with a 0.68 % increase in the local material budget, will be positioned in front of the ladder on adjacent C-frames to blow cold air onto the exposed sensor surface. Each station will have two perforated tubes on either side of the beam pipe as shown in Fig.1. Simulations have been conducted to optimize the size and number of holes in the tubes, with a tube inner diameter of 3.5 mm and a shell thickness of 0.25 mm. Each tube features 16 equidistant holes with a pitch of 14 mm, and the number of holes remains constant regardless of the ladder length [3].

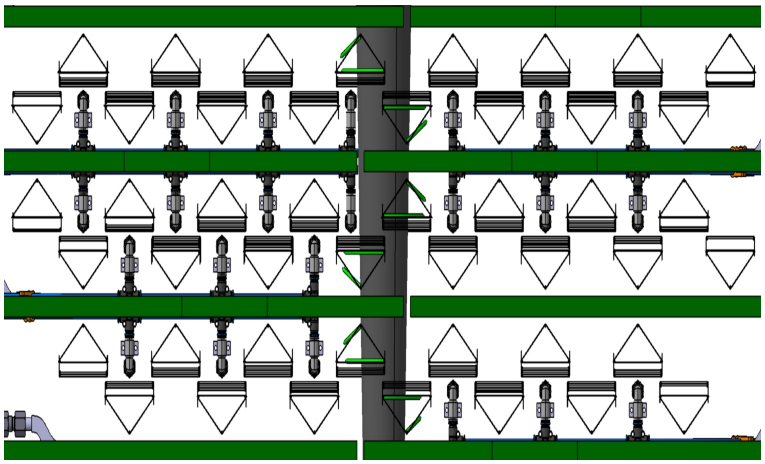

Figure 1: Top view of the STS ladder assembled on the C-frame with perforated tubes blowing the cold air

Since active cooling using perforated tubes has been optimized for the innermost sensors, with 20 x 20 cm^2 area, it is important to determine the required airflow rate for sensor cooling. Therefore, the airflow passing through the perforated tube was optimized to avoid thermal runaway, with respect to power density varying with sensor temperature as illustrated in the plot depicted in Fig.2. The parabolic curve in the plot indicate the heating power variation with sensor temperature [4]. The different colors indicate the cooling power achievable with the given perforated tube geometry at various airflow rates ranging from 20 L/min to 40 L/min when the gas is at -10°C.

The plot demonstrates that higher flow rates offer a larger margin from thermal runaway. By considering the optimal flow rate of 30 L/min passing through the perforated tube, sensors can still be operated at -10°C having sufficient margin from thermal runaway. However, it should be noted that excessively high flow rates in close proximity to the sensors can result in unwanted vibrations, which may interfere with the tracking reconstruction software and consequently impact the detector's momentum resolution.

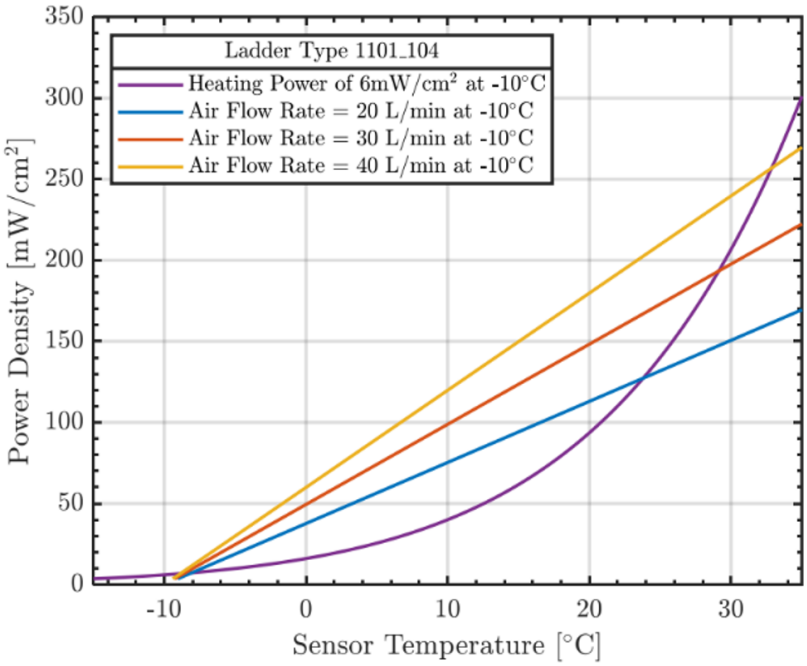

Figure 2: Thermal runaway plot showcasing the variation of sensor temperature with heating power at -10 °C

To assess the impact of vibrations on sensor stability, simulations were performed, specifically focusing on the inner region of central Au + Au collisions at 10 AGeV, as it is expected to have high rate. This investigation aimes to provide valuable insights into the influence of vibrations on the occurrence of ghost or fake hits and overall performance of the STS. To assess the impact of vibration on the sensors, simulations has been conducted using the STS hit-producer [5]. By introducing controlled random shifts to hits associated with the sensors, the resulting shifts in module positions were calculated to get an idea of the impact of vibration on sensors.

Preliminary results indicate that vibrations in the modules significantly impact the possibility of fake hits and can be summarised as:

1. No vibrations: It has been observed that without vibrations, the likelihood of fake hits is approximately 0.053 % (around 22.34 tracks per event). This indicates that vibrations play a crucial role in generating false signals and misidentified tracks within the detector system.

2. Moderate vibrations: When vibrations of around 1 μm are introduced in the XY direction (3.7 μm in Z), there is a slight increase in the likelihood of fake hits to 0.054 % (around 22.58 tracks per event). This demonstrates that even relatively small vibrations can contribute to the generation of false signals, impacting the accuracy of track reconstruction.

3. Higher vibrations: If the amplitude of vibrations is increased further to 10 μm in the XY direction (37 μm in Z), lead to a significant rise in the likelihood of fake hits. In this scenario, the likelihood increases to 0.234% of fake hits, corresponding to approximately 121.22 ghost tracks per event. This represents a substantial 23% increase compared to the absence of vibrations, emphasizing the detrimental impact of higher vibration levels on the detector's performance.

These results highlight the importance of minimizing vibrations in the sensor modules to minimise the occurrence of fake hits to aim for good particle tracking. Based on these results, it is imperative to check for the magnitude of vibrations generated in the sensors after the airflow in the perforated tube is set to 30 L/min.

2 Preparation of ladders to be tested under air flow

The inner region of STS comprises of two ladder types: ladder with central opening to accomodate the conical beam pipe [6] and standard ladders located in close proximity to the central ladders without cut-outs. In order to experimentally assess the impact of airflow-induced vibrations on the sensors, test setups were established for both ladder types. These setups specifically targeted the region, where radiation dosage is most pronounced. A comprehensive overview of the ladder structure and fabrication can be found in Technical Note [7].

Before assembling the ladders with the modules, optical inspection was conducted to evaluate the damping characteristics of the ladder structure itself. To determine the stiffness of the ladders, prototype ladders with and without cut-out have been assembled by ICM composites. While the ladders were fabricated, simulations were conducted to ensure that the ladders remained adequately stiff with minimal material used, specifically the central ladders. Three ladders were optically inspected: standard ladder without cut out and two ladders with different cutout lengths having diameter of – mm and 83mm, as depicted in Fig. 3.

Figure 3: Prototype of different ladder types

The central ladders, in comparison to the standard ladders, will experience a higher load due to the presence of the cut-out, resulting in approximately twice the elongation compared to the normal ladders. This indicates that the central ladder might exhibit reduced stiffness, allowing for larger deformations. To assess the characteristics of the bare ladders, they were placed on support structures and subjected to random loads equivalent to the weight of the sensors and micro-cables (approximately 110 g for 10 modules). Fig.4, shows an example of a central ladder with an 83 mm diameter, and it is evident from the figure that the ladder is no longer perfectly straight, displaying noticeable deviation from its original form.

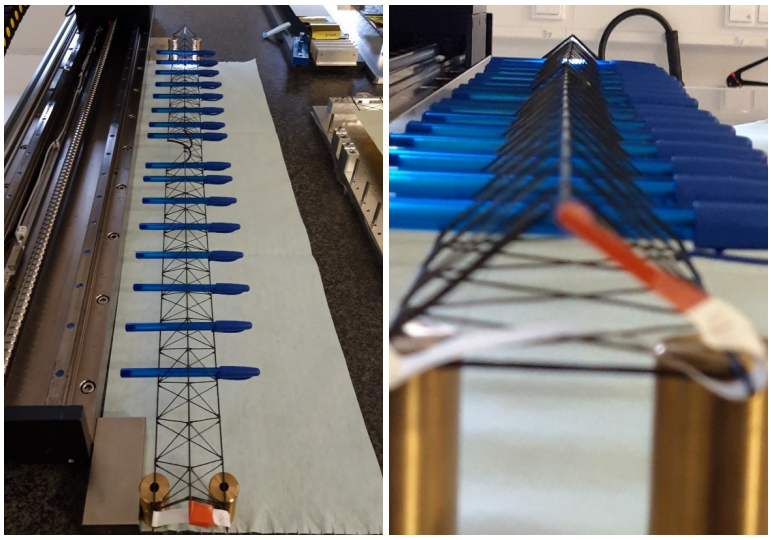

Figure 4: Central ladder fixed on support for optical inspection with load equivalent to weight of sensors and micro-cables

The results for all three ladders are presented in the plots shown in Fig. 5, illustrating the deviations in the y and z axes from their nominal positions. Under the influence of a normal load equivalent to the weight of the sensors and cables, the central ladder with the larger cut-out (considered as the worst-case scenario) exhibits a z-direction deviation of approximately 2.8 mm and a y-direction deviation of 1.59 mm. The y-direction deviation is of particular concern, as any movement in the sensor position along the y-axis, resulting from the applied load, could interfere with accurate particle tracking. In contrast, the standard ladder demonstrates minimal deviation in the y-direction, and only slight sagging is observed in the z-direction (0.3 mm).

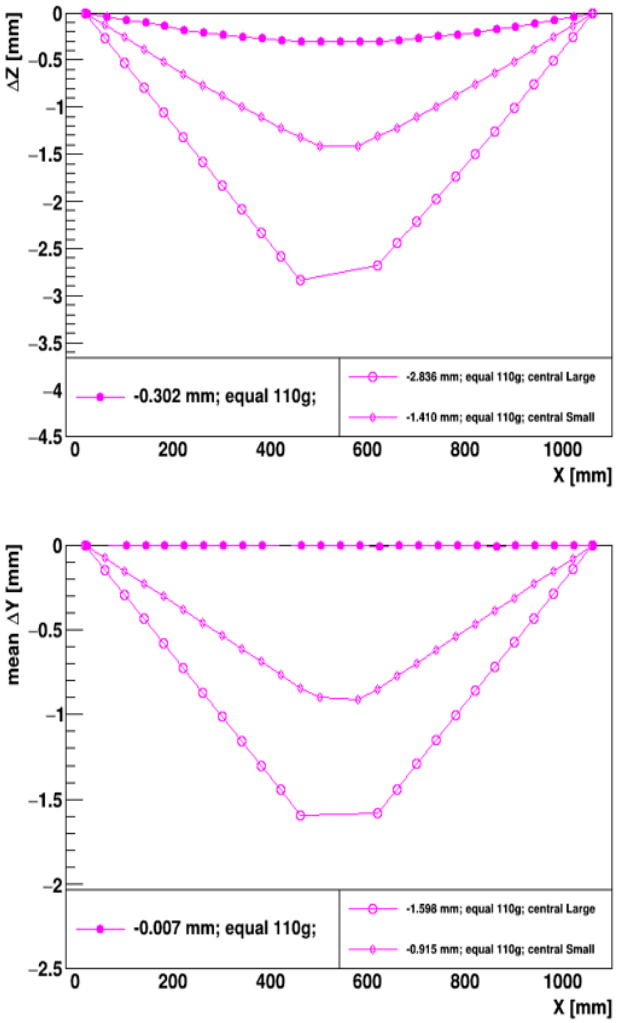

Figure 5: Plots showing the deviation in ladder structure under load in (a) z direction (b) y direction

After the optical inspection of ladder, it was also challenging yet interesting to optimise the impact of ladder being fully assembled with modules and to check how precisely they can be assembled under the load of the module. It is important to note that the mounting precision of 100 μm plays an important key role in particle tracking [9]. The deviation in sensors position, particularly in the XY direction, can result in degraded spatial resolution, compromised track reconstruction algorithms, reduced tracking efficiency. Also, the increased uncertainties due to multiple scattering, combined with misaligned sensors, can make it more challenging to accurately determine the original trajectory and momentum of the particle, leading to less precise tracking results. Therefore, it is crucial to obtain precise sensor alignment for maintaining the desired performance of the track based alignment software. Apart from mounting precision, the another reason for misalignment in sensor positioning is the vibrations produced in sensors because of

air flow. Therefore, to understand the impact of airflow induced vibrations, two specific types of ladders have been assembled, standard ladder as well as the ladder with wider centre opening with diameter of 83 mm.

2.1 Standard ladder

To achieve the sensor mounting precision within 100 μm, a well-defined assembly technique was developed and tested. Since the maximum number of modules a STS ladder can have is 10, therefore, a full size ladder with 10 non-functional modules was constructed, as shown in Fig.6. This is the first full-size ladder assembled which served two purposes: familiarizing with the precise module mounting procedure and providing an appropriate platform for conducting vibration measurements.

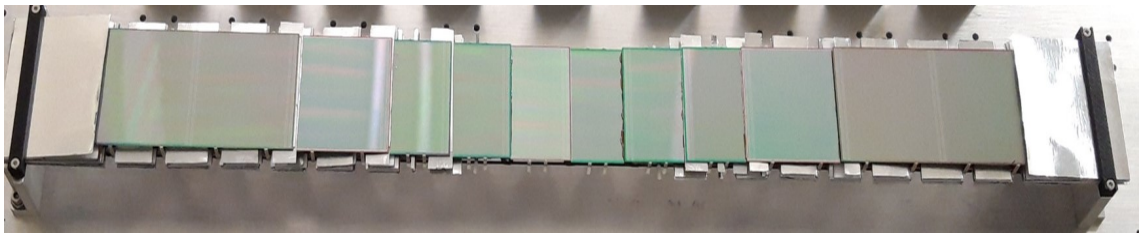

Figure 6: STS ladder assembled with 10 non- functional modules (i.e., modules with sensors and micro-cables with the shielding without any Front End Boards (FEBs))

After the ladder is assembled, an optical inspection is performed to evaluate the accuracy of sensor's placement. To achieve this, a camera-based proximity-focus measurement setup on a granite table with XYZ motor stage is used [8]. The 3-D position of the sensors is determined from alignment marks on their surface. The plot in Fig. 7 illustrates the deviation of these markers from their nominal position (in x, y, and z coordinates). The highlighted region indicates that all the sensors are within the required precision of 100 μm. To ensure accessibility for detector alignment, the survey data for all assembled ladders will be systematically stored in a database. Optical inspection is planned to be performed for all the ladders, prior to their mounting on the C-frame, to get familiar with the idea of how much can be the effect of mounting on the particle tracking.

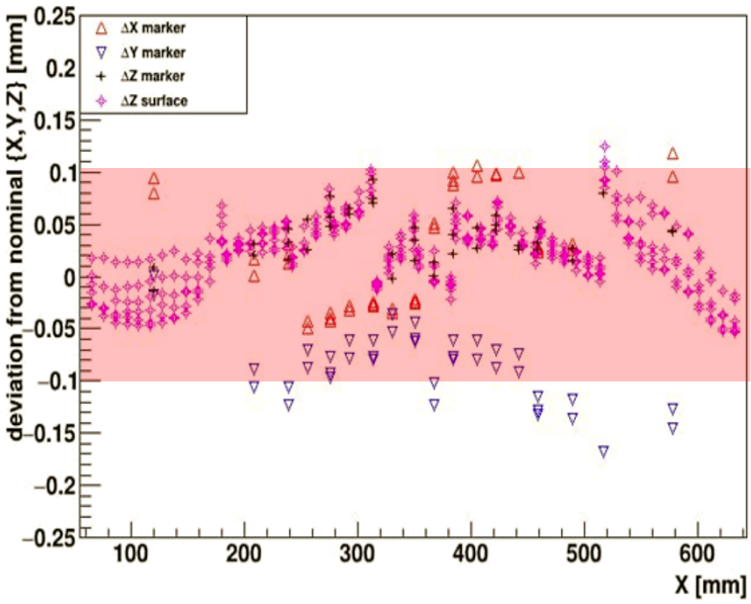

Figure 7: Measurement of markers on the sensor surface and deviation of markers from the nominal position has been plotted along the length of the ladder

2.2 Central ladder

For the assembly of a central ladder, dummy modules made of silicon wafers were used instead of actual sensors connected by micro-cables. Assembling the central ladder has been a challenge in itself, as central ladders exhibited more sagging compared to the standard ladder. To prevent sagging during assembly, gauge blocks (shown in Fig.8) were mounted underneath the ladder close to the cut-out section. Additionally, the cut-out itself required extra support to ensure it remained fixed in its position after the ladder was cut and glued to the bearings, enabling it to fit into the beam pipe. Therefore, a special tool was designed to support the cut-out region during assembly, as depicted in Fig.8, ensuring the ladder was centered correctly.

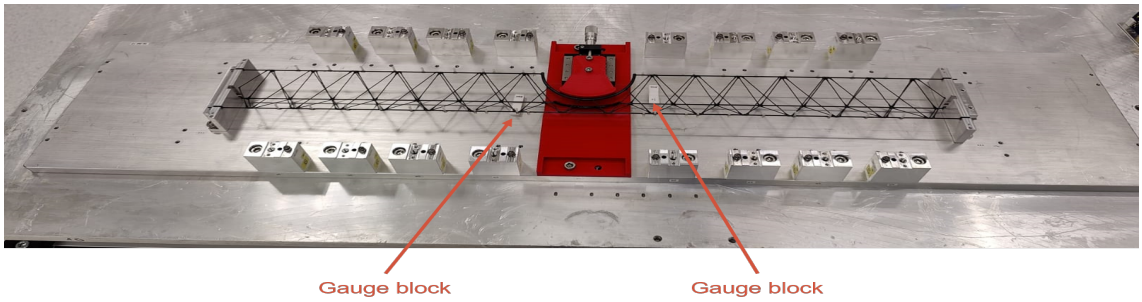

Figure 8: Assembly of prototype of central ladder using specific designed tools and gauge blocks to avoid sagging in the ladder during the assembly

To fulfill the objective of testing the central ladder under airflow and comparing it with vibrations generated in the standard ladder, the central ladder was resized to match the length of the standard ladder (i.e., Ladder type 12 with a length of 620 mm). The silicon wafers used during the assembly had a thickness approximately 30 % greater than the actual STS silicon sensors (320 μm) due to the unavailability of the actual sensors. Nevertheless, comparing the two ladders would provide insights into the amplitude of vibrations under airflow.

3 Mechanical stability of STS ladders

To accurately measure vibrations in the ladder, it becomes imperative to evaluate the stability of the assembled ladder itself. The design of STS ladders is optimized to minimize deformations under load, but it needs to be verified for stability under realistic loads. Load tests are important for STS ladders as they bear the weight of modules during assembly, and must withstand mechanical loads from sensors and micro-cables (nearly 10-12 g per module). Additionally, in regions with high radiation where sensors are exposed to direct airflow, ladder deformations may occur, potentially affecting the position and alignment of the sensors.

The degree of ladder deformation is influenced by external factors like air flow, environmental conditions, and the ladder's eigen frequency, which refers to its natural frequency of vibration. When the ladder's eigen frequency aligns with external forces, resonance can occur, leading to substantial vibrations and significant deformations. To prevent structural damage, it is crucial to ensure the ladder's eigen frequency is different from resonant frequencies caused by external forces. This ensures stability, prevents significant deformations, and enables accurate position measurements and sensor alignment.

To understand the behavior of ladder, two identical standard ladders, similar to the one depicted in Fig. 4, were assembled. One ladder was dedicated to identify the eigen frequency, while the other was used to measure ladder vibrations induced by airflow. This exploration aimed to acquire the importance of vibration intensity for smooth operation of track-based alignment software and to check whether the airflow could excite ladder's eigen frequency.

3.1 Eigen frequency measurements of STS ladder

To measure the eigen frequency of STS ladders, two ladders were sent to University of Oxford, Great Britain, within the EU project AIDA2020 [10], where a facility with realistic mechanical loads is used to measure the resulting deformations of the structure. To perform the measurements, a shaker table optimized for low vibration levels in typical static environment is used. The shaker table was driven by a 10" speaker, and MEMS-based accelerometers (ADXL 325) were used to monitor the level of vibrations with an acceleration noise density of 250 μg / $\sqrt{Hz}$ (1 g = 9.8 m/s^2). The main aim of using the shaker table was to analyze and measure the eigen-frequency of the ladder, so that during the measurements of the STS ladder under flow, it could be cross-checked if there is any effect of air flow on ladder's eigen-frequency.

Two accelerometers, referred to as left and right accelerometers, are mounted on both ends of the shaker table. Before performing any measurements with the shaker table, spectra for both the accelerometer were obtained as can be seen in the graph in Fig. 9, where peak acceleration is plotted with respect to the frequency in x, y and z direction. From the accelerometer spectra, it can be observed that the rocking mode of the table is around 42 Hz and any excitation during the ladder scan around this frequency range can be avoided since that is solely coming from the table. Also, the coherent acceleration peaks are observed at both the accelerometers at around 320 Hz in response to the excitation from the motors. It is assumed that this is the 2_{nd} mode of the table. Since the displacement at these frequencies are small, therefore, these excitation's do not add up to the displacement data of the ladder.

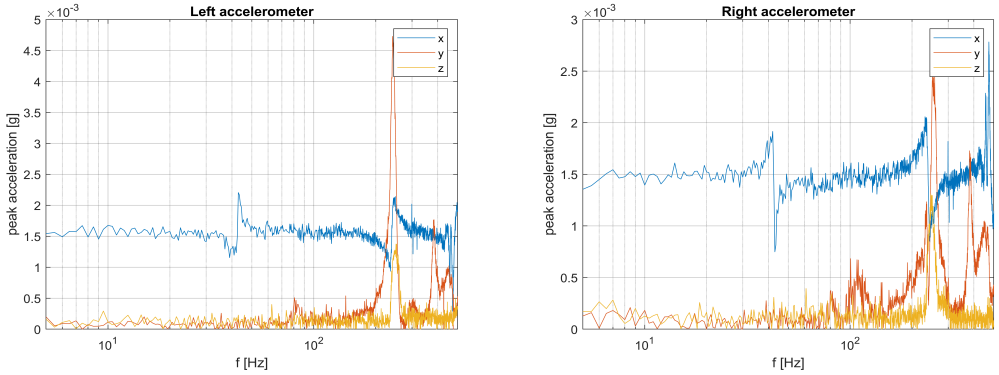

Figure 9: Plots showing the data from both the accelerometers placed at either end of the shaker table

To measure the eigen frequency of the ladder, it is mounted on the shaker table. Capacitive sensors were used which enables displacement measurements of the surface under scan. These sensors worked effectively with the conductive and reflecting surface of silicon. Three capacitive sensors were used to measure the displacement in the ladder. Two sensors were fixed close to the supported end of the ladder, i.e., ladder bearings to measure the displacement in the table due to the accelerometers. The other one sensor was used to track the movement of ladder in the middle, as illustrated in Fig. 10.

The data obtained from the capacititve sensors consists of approximately 250 samples recorded at a sampling frequency of 2 kHz, capturing the amplitude (or RMS) of a sine wave with the excitation frequency. The resulting data from the table sensors is plotted in Fig. 11, illustrating that both the sensors close to the bearings show an excitation in peak somewhere close to 220 Hz. The spectra from these sensors are then averaged to obtain the excitation coming from the table, which can be later subtracted from the measurements taken from the middle sensors.

The other capacitive sensor was positioned at a distance of 510 mm from the fixed bearing of the ladder, to scan the displacement in the middle of the ladder. The averaged displacement for the table sensor as well as for the middle sensor for ladder assembled with modules is shown in the plot in Fig. 12. From the plot it can be observed that the first eigen frequency of the ladder assembled with sensors and micro

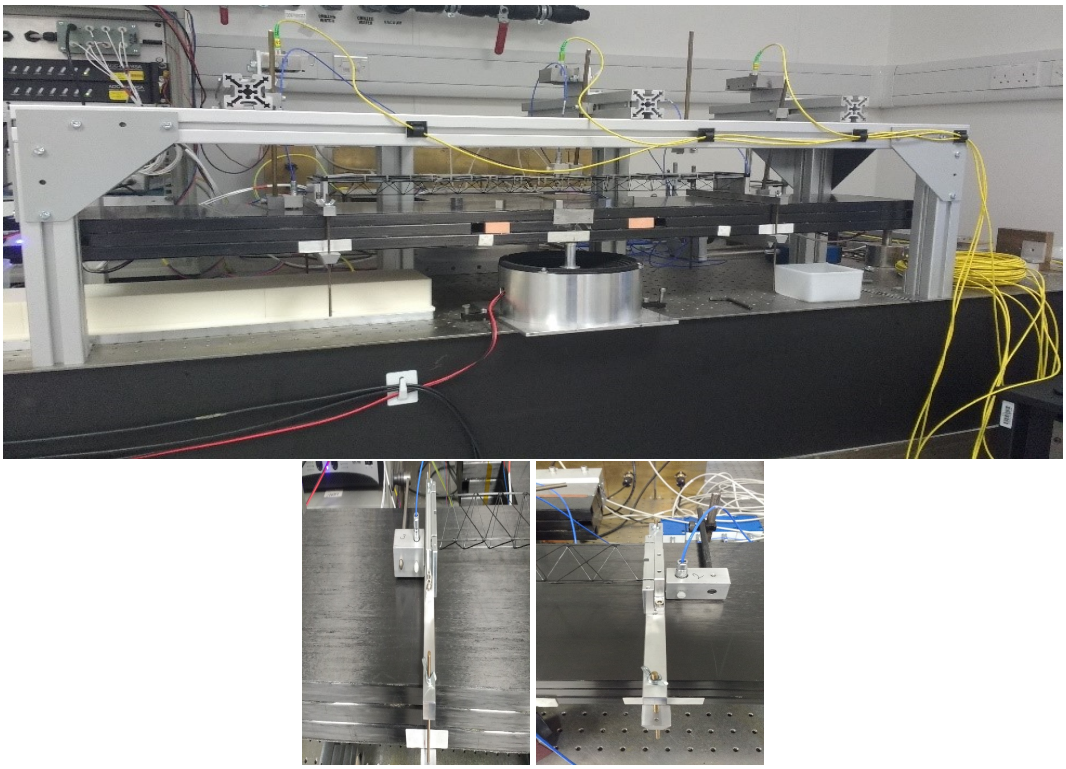

Figure 10: Top image: Assembled ladder mounted on the shaker table with 3 capacitive sensors, bottom left: capacitive sensor positioned close to fixed bearing, bottom right: capacitive sensor positioned close to floating bearing

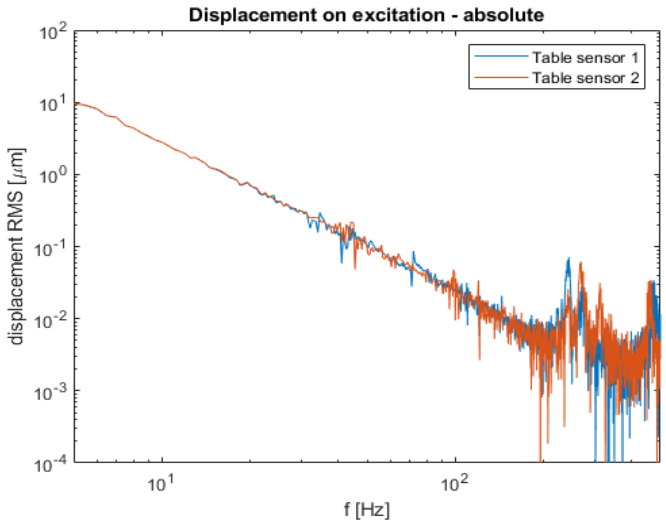

Figure 11: Frequency vs RMS plot of capacitive sensors close to the bearings, the average of these two spectra give the displacement of the table

cables, is around 67 Hz. Now it needs to be investigated with the air flow if this frequency is excited with the airflow.

3.2 Vibration under air flow

Since air cooling is necessary to minimize electronic noise and effects of radiation damage in the innermost sensors, achieved by using a thin carbon fiber tube with small evenly distributed holes to blow cold air on the sensors. However, the flow can induce turbulent air flow around the ladders, resulting in

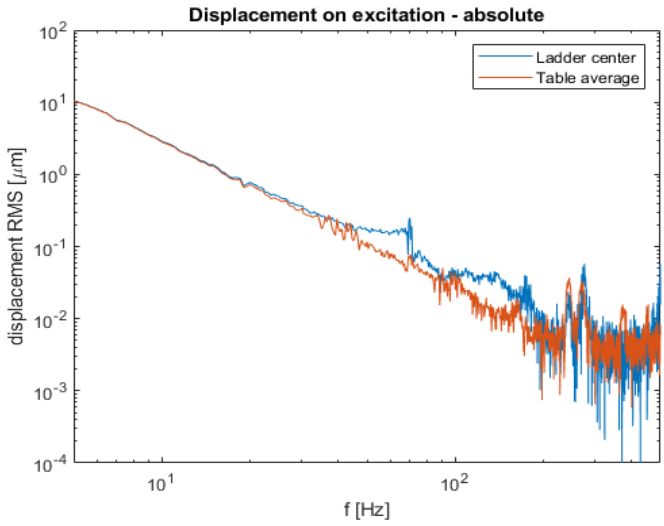

Figure 12: Frequency vs RMS plot showing the spectra for fully assembled ladder with the middle sensor used for scanning of ladder and the averaged measurements from the sensors close to bearings showing the displacement of table

vibrations that may affect the accuracy of track-based alignment software. Therefore, a testing procedure was optimized to evaluate the impact of airflow on the ladder and sensor vibrations.

To ensure the stability of the ladder, a customized aluminum baseplate was used which is mounted onto an optical bench with vibration isolators to minimize floor vibrations. The ladder itself was mounted onto the baseplate, while a perforated tube was attached to faciliate the airflow for sensor cooling. To cover the ladder, an enclosure has been prepared around the ladder, except for the front section that provided access to the sensor's surface as can be seen in Fig. 13.

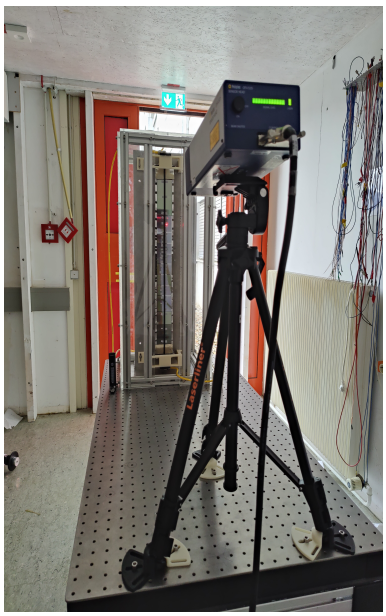

Figure 13: Set-up showing a ladder fixed to the optical bench covered in an enclosure with a perforated tube connected to the flow meters along with the fixation of laser head on the tripod stand

Precisely positioned in the center of the ladder, the perforated tube was connected to 3D printed connector holders, and leak-tight connections were achieved with Swagelok connectors. For measuring the volumetric flow of gas, FLK 2216 Acrylic variable area flow meters [11] were used. These flow meters operate based on the principle of variable area and are connected to the swagelok connectors of the

perforated tubes.

To measure the displacement in sensors under the air flow, a Laser Doppler Vibrometer (LDV) is used. It provides a convenient way to perform non-contact measurements of vibrating object. These vibrometers relies on the doppler effect to measure the velocity of a moving surface. This effect is produced by the frequency shift that occurs when light is scattered by a moving surface, and is detected using an interferometer. The interferometer works on the principle of optical interference, where two coherent light beams with distinct light intensities I_1 and I_2, overlap. The resultant intensity is written as:

$$I_{tot} = I_1 + I_2 + 2\sqrt{I_1 I_2 cos\frac{[2\pi(r_1 - r_2)]}{\lambda}} \tag{1}$$

where, r_1 and r_2 represent the distances from the source of interference to the respective locations where the intensities I_1 and I_2 are measured.

The laser vibrometer employs a Helium Neon laser with a frequency of 4.74 x 10^{14} Hz and a wavelength of 633 nm. The laser beam is split into two parts, the measurement beam and the reference beam, using a beam splitter called BS1. The measurement beam is directed through another beam splitter, BS2, and then focused onto the object being measured using a lens. As the object moves parallel to the laser beam, the frequency of the incident beam undergoes a shift, which causes intensity modulation of the recombined beam due to interference. This frequency shift is known as the doppler frequency shift, denoted as f_d, and can be expressed as

$$f_d \propto 2v_s\lambda \tag{2}$$

where v_s is the velocity of the surface and λ is the wavelength of the laser beam. The light that is scattered backwards is redirected by BS2 towards BS3, where it combines with the reference beam. The resulting combined beam is directed towards a photodetector which converts the optical signal to an electrical signal, generating an interference pattern between the measurement and reference beams as shown in Fig. 14.

To ensure precise measurements, the scanning head of the laser sensor was mounted on a tripod stand and attached to the screws of the optical bench to allow stability of laser during the measurements Fig. 13. The laser beam was focused on the surface of the object to achieve maximum laser focus while minimizing fluctuations. Therefore, it is crucial to determine the ideal distance between the sensor surface and the laser head, as it directly affects signal fluctuations. Moreover, the signal level plays a significant role in determining the signal-to-noise ratio (SNR) of the data. Higher signal levels result in better SNR, however, maintaining a stable signal level is equally essential. Generally, increasing the standoff distance results in decrease in signal level, with optimal standoff distance being closer to the point of maximum visibility. This visibility maxima determines the standoff distance at which the signal level reaches its peak. Therefore, the optimal standoff distance is given by the equation:

$$D = 234 + (n.l) \tag{3}$$

Where, D is the optimal standoff distance, n = 0, 1, 2, ..., l is visibility maxima = 204 mm

The dependence of signal level on the standoff distance can be observed in Fig. 15, where the signal level remains consistently high at the visibility maxima. The visibility maxima for OFV 525 laser is approximately 642 mm, as per the values mentioned in the manual. Hence, the ladder is positioned at a distance close to 642 mm from the laser head.

Once the setup is assembled, measurements were performed using LDV and accompanying VibSoft

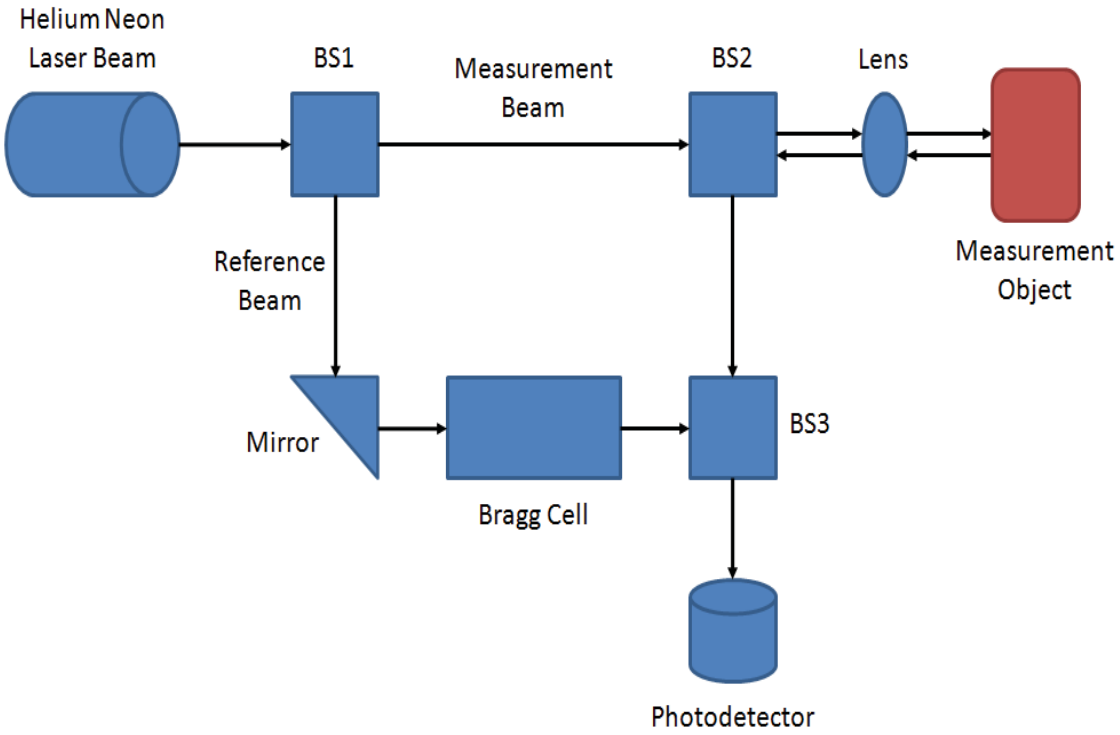

Figure 14: Schematic of laser doppler vibrometer

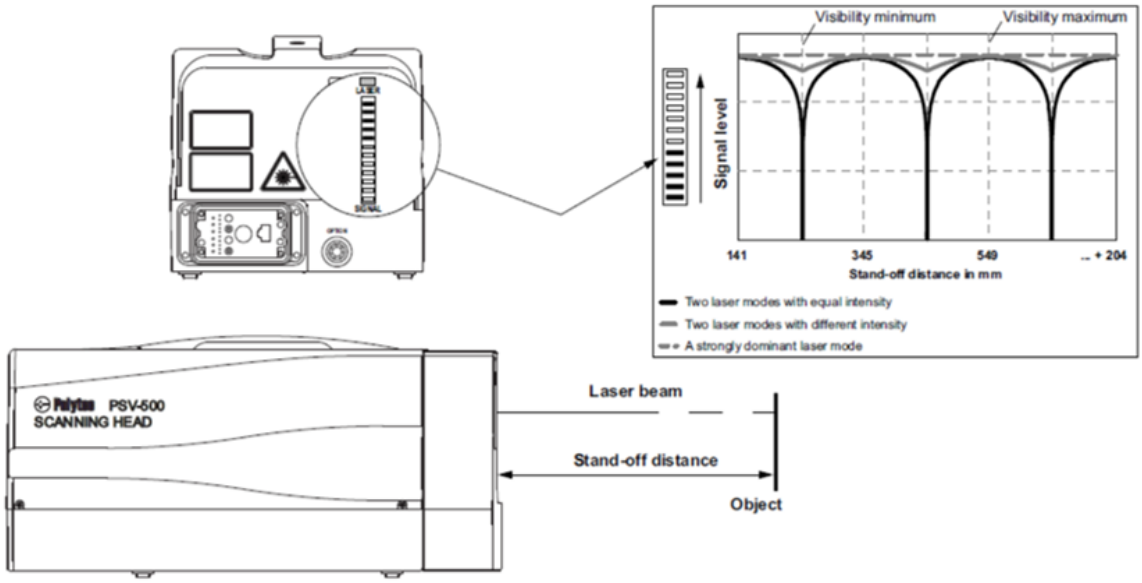

Figure 15: Optimization of stand off distance between laser sensor and the object under measurement

software. The software enables data acquisition, signal decoding, data display, and function generation by integrating a data acquisition board in the computer. The software simplifies and streamlines data analysis, making it easier to interpret complex vibration signals. To perform the measurements, laser is connected to vibrometer controller and a junction box as shown in the bloack daigram in Fig. 16. The junction box acts as an interface for the inputs and outputs of the vibrometer signal. To acquire vibration data, the appropriate measurement settings are selected in the VibSoft software which includes, general settings to choose between FFT or time signal, define the frequency range, specifications for the type of window to be used for signal processing and followed by data acquisition process. The software collects

the vibration data from LDV and save it in a file format that could be used for the analysis.

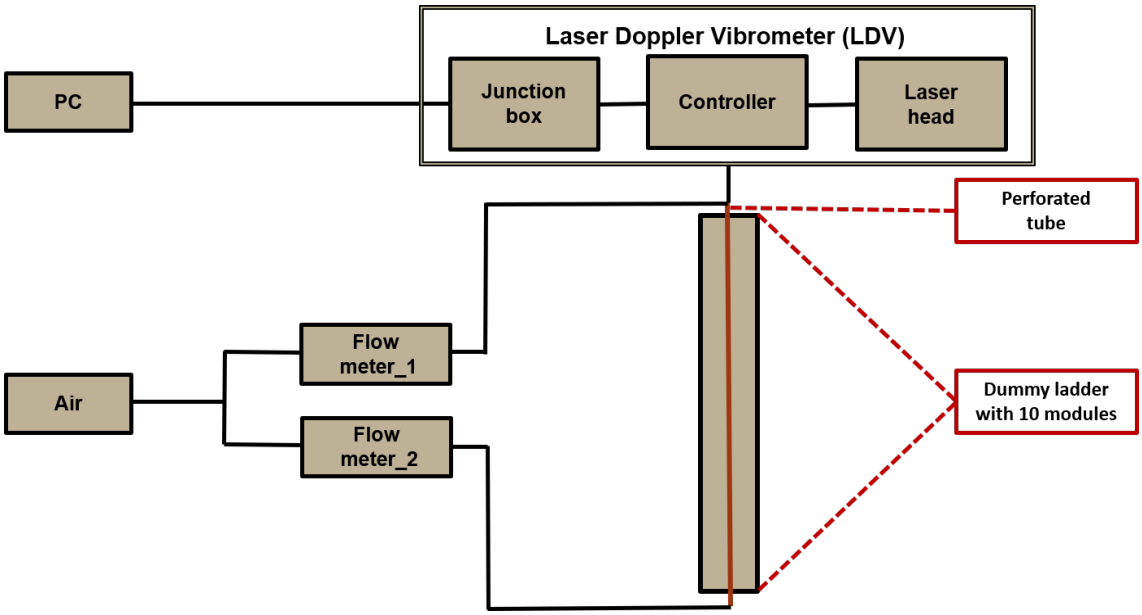

Figure 16: Block diagram of the setup with ladder as well as LDV components

The optimal air flow acquired from the simulations is expected to be around 30 L/min, hence measurements were taken for 20 L/min, 30 L/min and 40 L/min respectively. However, these measurements also includes the contribution of background along with the flow measurements. Furthermore, due to the limitation of having only one vibrometer, the primary challenge was to segregate the background signal from the flow measurements.

To separate the background from the flow measurements, a two-step approach was employed. Measurements were first recorded with the flow switched on, and then without disturbing the setup, another set of measurement was taken with the flow switched off to obtain background measurements. These background measurements were subsequently subtracted from the flow measurements to isolate the true flow signal, enabling more accurate flow measurement.

It was anticipated that the highest level of vibrations would occur in the vicinity of the perforated tube. As such, the amplitude of out-of-plane vibrations was measured at various points along both sides of the perforated tube, regardless of the size of the sensor. Fig. 17 (left) illustrates a schematic of a 6 x 6 cm^2 sensor with strategically selected measurement points to capture the effects of vibrations near both layers of L-legs and in the middle of the sensor between the L-legs where vibrations were expected to be prominent. The measured points were averaged to obtain an overall assessment of vibrations across the entire sensor surface, as shown in Fig. 17 (right).

To evaluate the flow measurements at each point on the sensor, a total of 10 measurements were taken for each point after focusing the laser on the sensor. The first measurement served as the baseline and was recorded with no flow (0 L/min). Subsequent measurements were taken by varying the flow rates through the flow meters at 20 L/min, 30 L/min, and 40 L/min, respectively. The goal was to obtain two measurements per flow rate in order to enhance reliability through averaging. To measure the vibrations, one of the most common way is to measure the Power Spectral Density (PSD) spectra as they show how the vibration signal's power is distributed across different frequencies, helping analyze vibration amplitudes at specific frequency ranges. Therefore, PSD spectra for both the ladders has been analysed and amplitude of vibration has been obtained and compared.

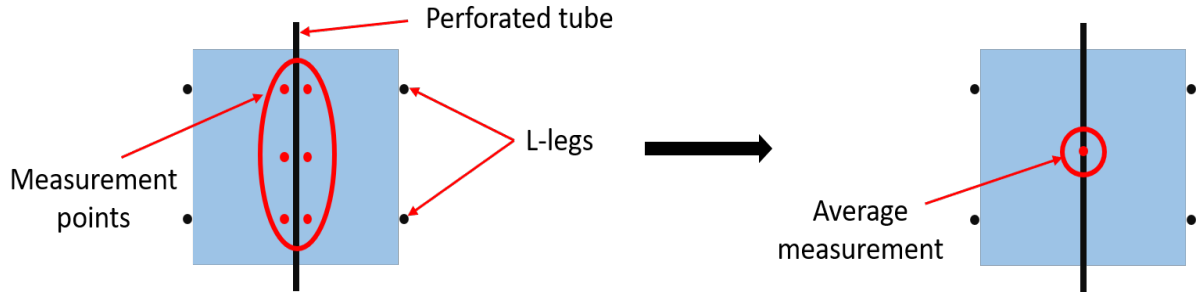

Figure 17: (a) Schematic illustrating the positioning of different measurement points on 6 x 6 cm^2 sensor surface (b) Averaging of measured points to obtain an overall assessment of vibrations across the entire sensor surface

3.2.1 Standard ladder

The Power Spectral Density (PSD) at different points as specified in Fig. 17 is measured for each sensor on the ladder at different air flows. The frequency vs PSD spectra data for the innermost sensor is shown in Fig. 18, where different colors on the plot represents the various flow rates passing through the perforated tube. From the plot, it can be observed that multiple peaks are being excited because of the air flow. The first peak appears at approximately 7-8 Hz, followed by another peak at approximately 20-25 Hz. However, it can be noticed that these peaks are also visible in measurements taken without air flow, indicating that they are likely due to external environmental noise rather than eigen frequencies of the sensor.

The subsequent peak that is excited due to air flow is expected to correspond to the first eigen frequency of the sensor. When compared with measurements conducted in Oxford, it can be inferred that the first eigen frequency of an assembled ladder (at 67 Hz) is not being excited, indicating that the ladder does not exhibit any damping effects due to airflow. This observation suggests the stability of the ladder is not compromised by the presence of airflow.

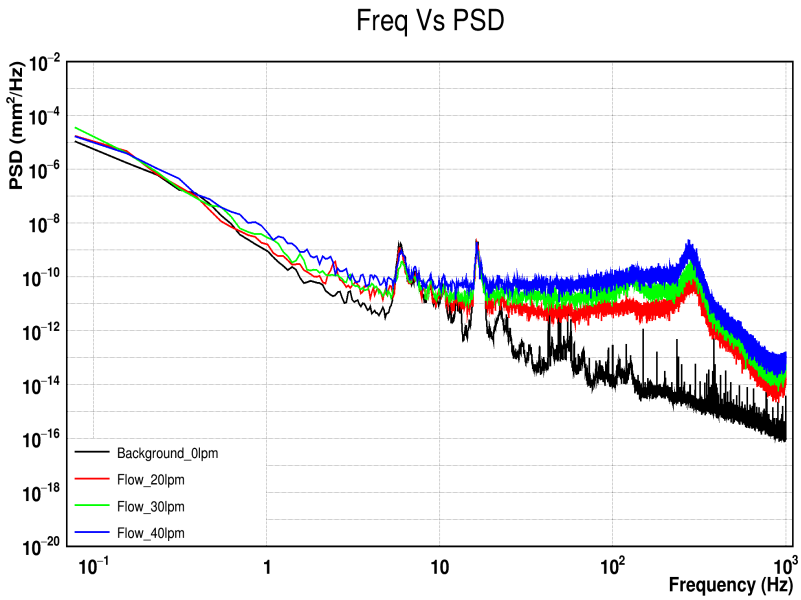

Figure 18: Frequency vs PSD spectra for different air flow for the inner most sensor

Taking a closer look at Fig. 18, it can be observed that lower frequencies, particularly those below 1 Hz, exhibit a more pronounced impact on the PSD spectra, which could be attributed to external background effects or seismic noise. This observation is consistent with measurements taken without airflow, suggesting that the observed vibrations may not be solely due to airflow-induced effects. Therefore, to

account for this, a soft frequency cut was applied during the calculation of vibration amplitudes, excluding frequencies below 1 Hz. This approach of applying a soft frequency cut below 1-2 Hz is commonly used in calculations for vibration analysis to minimize the impact of external factors.

To calculate the amplitude of vibration in the sensors, the RMS was calculated from the PSD spectra. The RMS value was obtained by integrating the PSD over the frequency range of interest i.e., $f_1 = 1$ Hz to $f_2 = 1000$ Hz and taking the square root of the integrated value, as shown in Equation 4.

$$RMS = \sqrt{\int_{f_1}^{f_2} PSD(f)\, df} \tag{4}$$

The RMS values for each sensor at different flow rates were then plotted, with distinct colors representing various flow rates, as depicted by the plot in Fig. 19. From the plot, it can be observed that higher flow rates lead to larger RMS values, indicating increased vibrations. Also, the middle sensors, particularly +3 and -3, exhibit more pronounced vibrations compared to other sensors which is because the holes of the perforated tubes are closest to these sensors.

For the required cooling of STS, the optimal flow rate of 30 L/min was found to be sufficient to cool down the innermost sensors [3]. The plot indicates that at this flow rate, the maximum amplitude of out of plane vibrations is estimated to be around 1 μm. This observation suggests that vibrations in the sensors will not adversely affect the particle tracking, and the alignment software can be safely utilized without any detrimental effects.

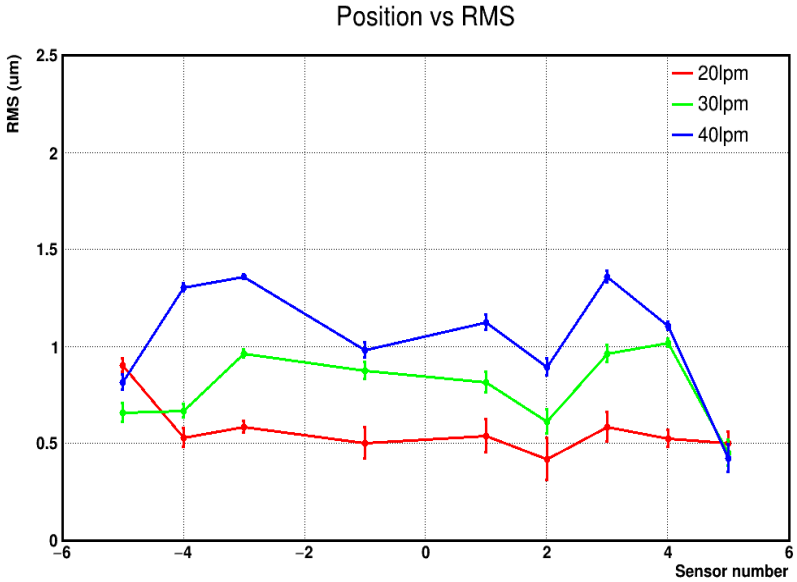

Figure 19: Plot showing RMS value for each sensor, where sensor number are shown on the x-axis and RMS is plotted on the y-axis

Based on the observations that highlighted the maximum vibrations occurring in sensor 3 and sensor -3, the data presented in Fig. 19 depicts measurements taken when the airflow was switched on and measurement was taken, which does not fully reflect the realistic operating scenario of STS. During the operation of the STS, it is anticipated that the detector will be continuously subjected to cold airflow. To verify this scenario, a worst-case scenario test was planned, wherein the ladder setup was exposed to continuous airflow of 40 L/min (higher than the optimal airflow), and measurements were conducted for the critical sensors, i.e., sensor 3 and sensor -3. A total of 14 measurements were taken at different time intervals over span of 3 days, and the PSD spectra was plotted for both sensors. Fig. 20 shows the

spectra of the first and last measurements taken for both the sensors under continuous flow.

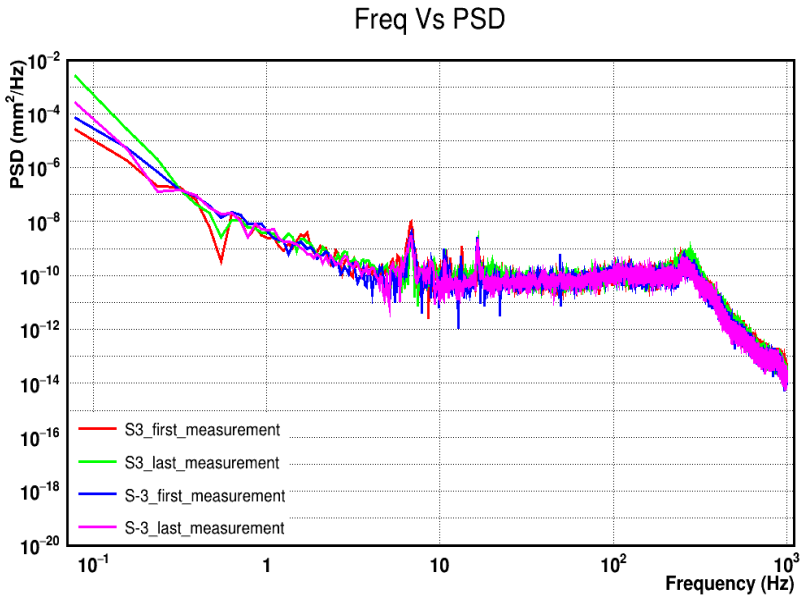

Figure 20: Frequency vs PSD spectra for the most critical sensors under continuous air flow

RMS values were calculated from the PSD spectra for the frequency range of 1 Hz to 1000 Hz, and RMS values were plotted for the different measurements of both sensors (See Fig. 21). The plots reveal that the RMS values for both sensors ranged between 1 μm to 2 μm. It can be noted that the error bars in the plots are relatively large due to lower statistics. Thus, it can be concluded that operating the inner sensors of the STS with a flow rate of 30 L/min will produce minimal vibrations leading to negligible impact on particle tracking precision.

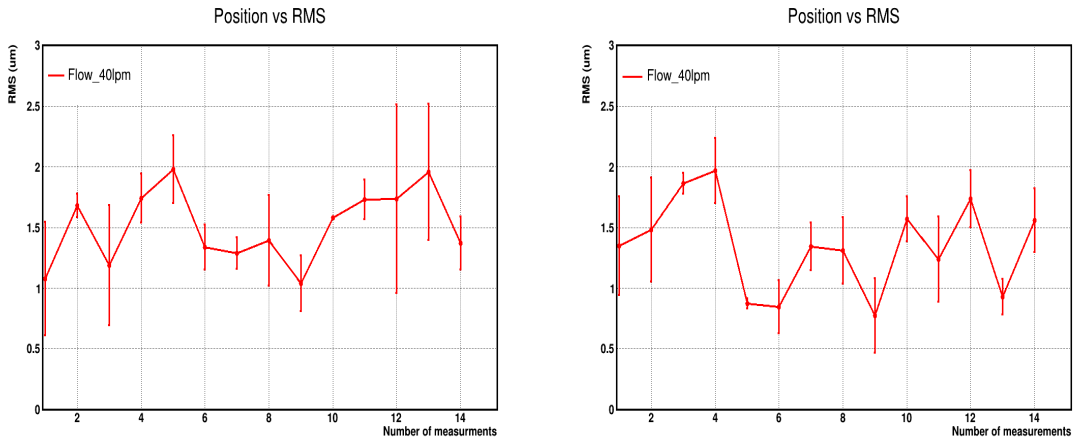

Figure 21: Position vs RMS plot for long term tests for (a) sensor 3 (b) sensor -3

3.2.2 Central ladder

The central ladder, once assembled, underwent testing to measure the vibrations caused by airflow on the sensors. In standard ladders, the perforated tube is positioned in the middle of the ladder whereas in the case of central ladder, due to the presence of beam pipe, the perforated tube is shifted by 2 mm, making the sensor surface on one side (closer to the tube) more vulnerable to vibrations. The measurements were performed following a similar procedure as explained in previous section, and RMS values were calculated for different air flow after subtracting the background and results have been summarised in Fig. 22.

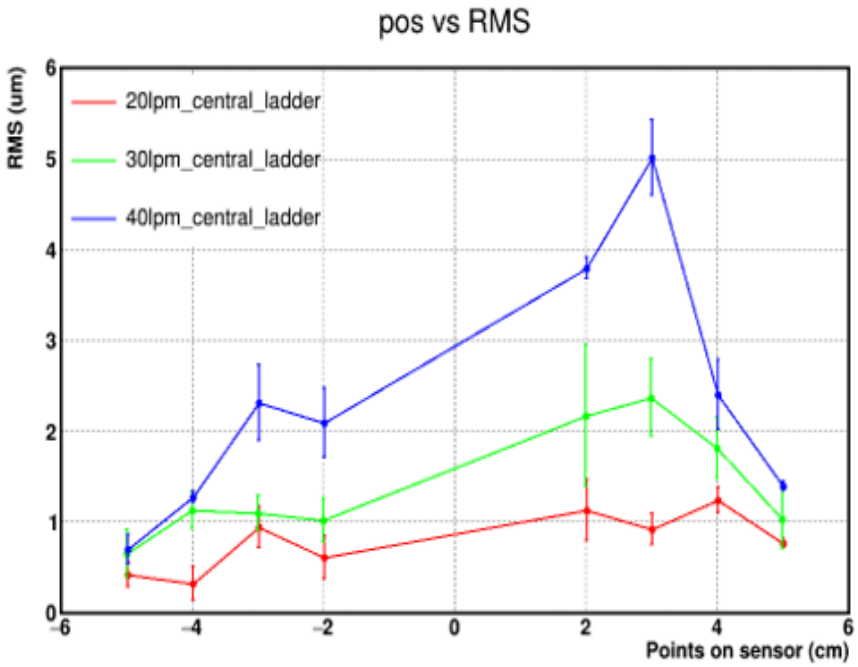

Figure 22: Frequency vs RMS plot for the central ladder under air flow

The plot indicates that positioning the perforated tube closer to the sensors (rather than in the middle of the ladder) leads to increased vibrations in the sensors. Despite the ladder being relatively less stiff, the amplitude of vibration for the optimal airflow rate of 30 L/min is around 2 μm, which is considered acceptable and not very detrimental to particle tracking. However, these results are preliminary, as the structure of central ladder is not yet finalised and the thickness of silicon wafers used was different from normal sensors. Nevertheless, these measurements provide an initial understanding of handling the central ladder and familiarize oneself with the expected vibration amplitudes. The ongoing simulations for a stiffer ladder version with improved reinforcement will be conducted, and the entire procedure will be repeated to obtain more conclusive results.

4 Summary and conclusion

This note investigates the impact of vibrations on the performance of standard and central ladders of the Silicon Tracking System of the CBM experiment. The findings highlight the influence of vibrations on the occurrence of fake hits in the sensors. The standard ladder demonstrates minimal vibrations when subjected to an optimal airflow rate of 30 L/min, resulting in a low possibility of fake hits ensuring good particle tracking. In contrast, the central ladder, situated near the beam pipe, is more susceptible to vibrations, leading to an increased possibility of fake hits. Further simulations and improvements in central ladder are being pursued to improve the stiffness and reinforcement of the central ladder to obtain more conclusive results. However, even under the worst-case scenarios considered, the amplitude of vibration in the weaker versions of the central ladder with a large beam pipe cut-out, remains within acceptable limits and does not impose have detrimental effect on the particle tracking.

References

[1] J. Heuser et al., eds. Technical Design Report for the CBM Silicon Tracking System (STS). Darmstadt: GSI Report 2013-4, 2013, 167 p. url: https://repository.gsi.de/record/ 54798

[2] V. Tesar. Impinging Jets, *In: Vortex Rings and Jets: Recent Developments in Near-Field Dynamics. Ed.*,by Daniel T. H. New and Simon C. M. Yu. Singapore: Springer Singapore, 2015, pp. 191–231. https://doi.org/10.1007/978-981-287-396-5_6.

[3] K.Agarwal et al., *STS Cooling Concept: Calculations and Simulations.* Technical Note CBM-TN-230xx. GSI, 2023.

[4] Private information from K. Agarwal .

[5] H. Malygina., *Hit reconstruction for the Silicon Tracking System of the CBM experiment.* PhD thesis. Frankfurt U., 2018

[6] J.heuser et al, *A full-size prototype of the STS beam pipe: design improvement, fabrication* In: CBM Progress Report 2022. Darmstadt: GSI, 2023

[7] J. heuser et al., *Production Readiness Review for the STS Carbon Fiber Ladders* Technical Note CBM-TN-19006. GSI, 2019

[8] E.Lavrik et al., *High-Precision Contactless Optical 3D-Metrology of Silicon Sensors.* Nucl. Instrum. Meth. A 935, 167-172 (2019)

[9] S.Das et al., *Track Based Alignment Procedure for CBM-STS Using Millepede II.* In: CBM Progress Report 2017. Darmstadt: GSI, 2017.

[10] *Advanced European Infrastructures for Detectors at Accelerators*, https://aida2020.web.cern.ch,EUHorizon2020GrantAgreementno.654168

[11] https://www.omega.de/pptst/FLK-2000-SERIES.html